Applied Surface Science 471 (2019) 222–230

Contents lists available at ScienceDirect

Applied Surface Science

journal homepage: www.elsevier.com/locate/apsusc

Full Length Article

Adsorption mechanism of typical oxygen, sulfur, and chlorine containing VOCs on TiO_2 (0 0 1) surface: First principle calculations

Asad Mahmood*, Gansheng Shi, Xiaofeng Xie, Jing Sun*

The State Key Lab of High Performance Ceramics and Superfine Microstructure, Shanghai Institute of Ceramics, Chinese Academy of Sciences, 1295 Dingxi Road, Shanghai 200050, PR China

ARTICLE INFO

Keywords:
VOCs
TiO_2 (0 0 1) surface
Formaldehyde
Methyl chloride
DFT

ABSTRACT

The photocatalytic degradation of volatile organic compounds has been gaining much interest in recent years to solve the long-standing problem of indoor air pollution. For this purpose, anatase TiO_2 and its derivatives are regarded as potential photocatalyst materials. Thus, we study the adsorption mechanism of selected volatile organic compounds such as formaldehyde, methyl chloride, and carbon disulfide on TiO_2 (0 0 1) surface using first principle calculations to comprehend their surface interaction and catalytic degradation in depth. The study suggests that formaldehyde interacts with TiO_2 (0 0 1) surface through chemical bonds that form a saddle-like structure exhibiting a high adsorption energy value (0.543 eV). It can be inferred that the fivefold coordinated Ti_{5c} and twofold coordinated O_{2c} atoms are the only adsorption sites on TiO_2 (0 0 1) surface. However, significant variations are observed for chloride and sulfur containing groups. For instance, the methyl chloride and carbon disulfide physisorbed on the surface of TiO_2 (0 0 1) without any chemical bond formation exhibits low adsorption energy values. The results are further confirmed by calculating the corresponding density of states, and electron density differences in all cases. This study provides a detailed investigation of various VOCs on the surface of TiO_2 (0 0 1), which provides further insight into the construction of photocatalytic materials for the photodegradation of VOCs.

1. Introduction

Volatile organic compounds (VOCs) in the indoor and outdoor environment present serious health risks as the majority of these pollutant gases are toxic and malodorous in nature [1,2]. VOCs are introduced into the environment from different natural and anthropogenic sources ranging from household products such as paints, pesticides, aerosol sprays, and wood disinfectants to building materials, biomass combustion, and furnishing [3–6]. The US environmental protection agency (EPA) has regulated around 300 VOCs because these gases can produce photochemical smog and are “carcinogenic-mutagenic-teratogenic” [7]. Ongoing revisions in the environmental protection agency codes for minimizing the VOCs hazards for workers in industries including cars and paints demand none to low concentrations of VOCs.

To this end, two strategies have been implemented to address this issue: (1) the capture of VOCs through physical or chemical adsorption, and (2) destruction and degradation of VOCs by various oxidation processes [8–12]. Among these, the photocatalytic oxidation method is proficient in removing hazardous organic contents from indoor environments [13]. Therefore, different metal oxide based semiconductor materials, for instance, CeOx [14], TiO_2 [15], CuMnO [16], $LaMnO_3$ [17], γ-Al_2O_3 [18], $Bi_2O_2CO_3$ [19] have been studied to design potential photocatalysts for the photodegradation of VOCs. The atomic arrangement and morphology are important features of the surface of a catalyst that can fundamentally influence its reactivity in surface catalyzed reactions [20]. For the most part, the presence of under coordinated atoms at the surface renders greater reactivity for these reactions.

Anatase TiO_2 (band gap = 3.2 eV) is a well-known photocatalyst exhibiting a tetragonal crystal structure with a space group of $I4_1/amd$ (D_{4h}^{19}) and measured lattice parameters of: a = 3.7845 Å and c = 9.5143 Å [21]. TiO_2 has been widely considered for various optoelectronic (refractive index $n_\omega = 2.561$, $n_\varepsilon = 2.488$) and photocatalytic applications due to its high electron mobility, good chemical stability, longer exciton diffusion length, and suitable band energy levels for many photocatalytic reactions [22–24]. Additionally, superior structural stability, low-cost, abundance, non-toxicity, and ease of production distinguishes TiO_2 among its counterparts, for example, ZnO, ZrO_2, CeO_2, SnO_2, CuO, and Cu_2O for optical and electronic applications [25]. In the polycrystalline powder form, various facets of

* Corresponding authors.
E-mail addresses: amkhan036@yahoo.com (A. Mahmood), jingsun@mail.sic.ac.cn (J. Sun).

https://doi.org/10.1016/j.apsusc.2018.12.017
Received 8 October 2018; Received in revised form 9 November 2018; Accepted 3 December 2018
Available online 03 December 2018
0169-4332/

TiO_2 exist, including (1 0 1), (0 0 1), and (0 1 0). The surface energy of TiO_2 (1 0 1) ~0.44 J/m^{12} is lower in contrast to (0 0 1) and (0 1 0) exhibiting a surface energy of 0.90 and 0.53 J/m^{12}, respectively [26]. In this way, under normal growth conditions, TiO_2 anatase phase grows in a tetragonal bipyramid shape, exhibiting a greater percentage of (1 0 1) surface. However, the Ti atoms (100%) at the (0 0 1) surface are undercoordinated (5-fold coordination; Ti_{5c}), which makes TiO_2 (0 0 1) surface more reactive in contrast to TiO_2 (1 0 1) surface where only 50% of the Ti atoms are undercoordinated. Consequently, the TiO_2 (0 0 1) surface is considered to be more appropriate for surface catalyzed reactions where the undercoordinated Ti_{5c} and O_{2c} atoms play an important role [27].

For the photocatalytic degradation of VOCs, adsorption of gas molecules is pivotal for interaction with the reactive species on the catalyst surface. The activity of a photocatalyst is predominantly associated with the absorption of light (photons), which causes the excitation of photoelectrons from the valence band (VB) to the conduction band (CB), thus, generating electron-hole pairs. These photoelectrons further produce reactive oxygen species (ROS), for example, $^{\cdot}OH$, $^{\cdot}O_2-$, and H_2O_2, which decompose and mineralize the organic compounds on the surface of photocatalysts [28,29]. These reactive radicals are generated according to the following reactions [30]:

$$TiO_2 + h\nu \rightarrow TiO_2\ (e^- + h^+) \quad (1)$$

$$H_2O + TiO_2\ (h^+) \rightarrow TiO_2 + {}^{\cdot}OH + H^+ \quad (2)$$

$$O_2 + TiO_2\ (e^-) \rightarrow TiO_2 + {}^{\cdot}O_2^- \quad (3)$$

Considering above, we systematically explore the adsorption mechanism of selected VOCs, including formaldehyde, methyl chloride, and carbon disulfide on TiO_2 (0 0 1) surface using first principle calculations. Formaldehyde (CH_2O), methyl chloride (CH_3Cl), and carbon disulfide (CS_2) are viewed as toxic VOCs containing aldehyde groups, chlorine, and sulfur atoms in their chemical structures, respectively. These VOCs are largely present in urban atmospheres. For example, formaldehyde is an imperative precursor material in the processing of various products including tissue fixative and embalming agent, biocide, disinfectant, drug testing, photography, and industrial resin production [31,32]. Methyl chloride has both natural and anthropogenic sources belonging to the haloalkane family which has been widely used as a refrigerant. A large amount of methyl chloride is produced naturally in the oceans by the action of sunlight on biomass and chlorine in the sea foam [33]. In any case, all chloromethane used in industry is produced synthetically. Similarly, carbon disulfide is considered exceptionally dangerous and is linked to both acute and chronic poisoning causing toxic effects such as neurofilamentous axonopathies [34]. Nonetheless, it is synthesized in the industry for different applications. It has been reported that the worldwide production of carbon disulfide surpasses one million tons per annum. The current daily exposure of 40 ppm has been reported for industrial workers; however, the recommended exposure is 5 ppm in Europe and 20 ppm in the United States of America [35,36]. Therefore, the adsorption configurations of these three VOCs on TiO_2 (0 0 1) surface are studied in this work to comprehend the interaction of these gases with TiO_2 (0 0 1) surface using first principle calculations. To contemplate the physical or chemical interaction with the TiO_2 (0 0 1) surface, it is of high importance to calculate the electronic structure of adsorbed molecules and evaluate various surface features that play a major role in the adsorption and decomposition of these VOCs. Additionally, we calculated the local density of states and electron density differences to further study the coupling of atomic states, and electron density rich and depleting regions. For this reason, various orientations were used to calculate the minimum energy configurations that were further used to calculate the local density of states and electron density differences. The current results can provide a theoretical basis for the photocatalytic degradation of organic pollutants in the air.

2. Computational details

The calculations were performed using generalized gradient approximation (GGA) to treat all electronic energy of exchange-correlation function implemented by standard Perdew-Burke-Ernzerhof (PBE) functions [37]. Additionally, an ultrasoft pseudopotential was used. In the first step, the calculation was performed for the bulk TiO_2 crystal structure in a 2 × 2 × 2 supercell, using valance electrons Ti: 3s, 3p, 3d and O: 2s, 2p utilizing a plane wave basis set and the cutoff energy of 400 eV. The lattice parameters for the bulk TiO_2 after structure relaxation have been calculated as a = 3.83 Å, c = 9.601 Å, with a k-point grid of (3 × 2 × 1), which are in good agreement with previously reported values (a_{exp} = 3.776 Å and c_{exp} = 9.486 Å) [38,39]. The anatase TiO_2 (0 0 1) surface is selected using (2 × 3) supercell, which provides a large enough surface to study the adsorption of formaldehyde, methyl chloride, and carbon disulfide. A vacuum of 20 Å was used to avoid the interaction between the slabs and to create a surface effect. Moreover, to account for the weak Vander wall forces (vdW) between the gas molecules and TiO_2 (0 0 1) surface, vdW D correction method (DFT-D framework) given by Grimme is used [40]. The surface cell was composed of 72 atoms, including 24 titanium and 48 oxygen atoms. The bottom two layers of the slab were fixed to their bulk position while the rest of the layers were allowed to relax. Moreover, periodic boundary conditions were used in a super cell using a k-points set of (2 × 2 × 1). The organic molecules were first optimized separately, and the optimization procedure is available in supporting materials (Section S1).

The convergence of total energy during electronic self-consistent iteration process was considered to be achieved when two iterated steps with energy difference less than 1.0×10^{-6} eV were observed. The adsorption energy (ΔE_{ads}) is calculated according to Eq. (1):

$$\Delta E_{ads} = (E_{Molecule} + E_{Surface}) - -E_{Molecule/surface} \quad (1)$$

where $E_{Molecule}$ is the energy of a molecule in the gas phase, $E_{Surface}$ is the slab energy without adsorption and $E_{Molecule/Surface}$ is the energy of the surface and molecule complex. Generally, the calculated positive value of E_{ads} refers to an exothermic process while a negative value recommends the endothermic process, which demonstrates the instability of the adsorption structure. To further comprehend the electronic structure and interaction of the gas molecules with TiO_2 (0 0 1) surface, we calculated the local density of states and partial density of states, demonstrating the mechanism of adsorption of the gas molecule on TiO_2 (0 0 1) surface in more depth.

3. Results and discussions

3.1. Anatase TiO_2 (0 0 1) surface

Fig. 1 shows the fully relaxed TiO_2 (0 0 1) surface, which has been used for the adsorption of selected molecules exhibiting different configurations. The surface is composed of 5-fold under-coordinated Ti atoms (designated as Ti_{5c}), 2-fold coordinated (designated as O_{2c}), and 3-fold coordinated (designated as O_{3c}) O atoms. The average bond length between Ti_{5c}—O_{3c} and Ti_{5c}—O_{2c} is calculated as 1.95 Å and 1.90 Å, respectively, which is in good agreement with previously reported values [41]. The respective bond angle for the bridge atoms Ti_{5c}—O_{2c}—Ti_{5c} is calculated as 138.7°. It has been reported that such a big bond angle at this site renders more surface tension to TiO_2 (0 0 1) surface [42]. The calculated small value of average bond length between Ti_{5c} and O_{2c} atoms (1.90 Å) in contrast to Ti_{5c}—O_{3c} (1.954 Å) suggests a strong Ti_{5c}—O_{2c} bond. The TiO_2 (0 0 1) surface analysis suggests Ti_{5c} and O_{2c} as active sites for adsorption. We used different adsorption modes for each molecule to attain minimum energy configurations.

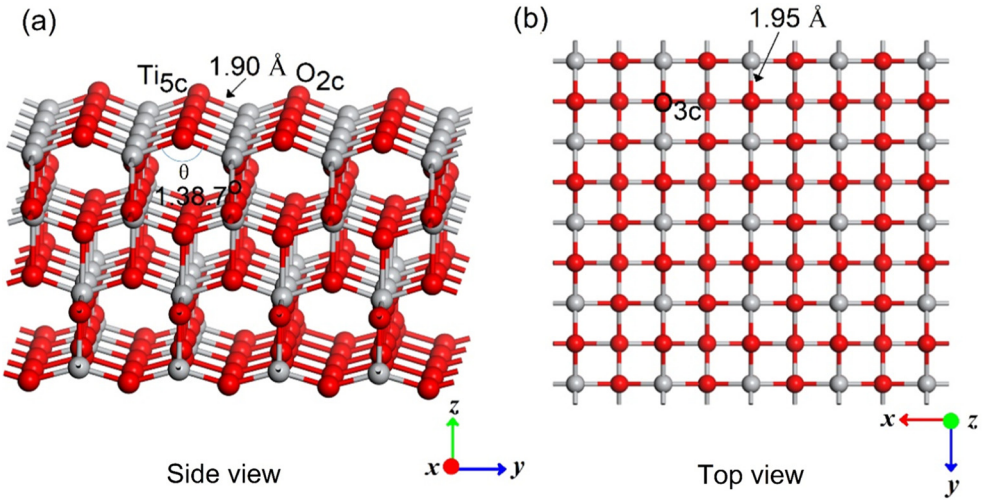

Fig. 1. Optimized structures of the (a) side view and (b) top view of anatase TiO_2 (0 0 1) surface. Ti and O atoms are labeled as light gray and red spheres, respectively. The bond length is Å.

3.2. Formaldehyde (FDH) adsorption

Initially, the formaldehyde molecule was relaxed to get a geometrically stable structure (Fig. 2). The respective highest occupied molecular orbitals (HOMO) and lowest unoccupied molecular orbitals (LUMO) are additionally given. After geometry optimization, the length of C═O and C−H bonds in formaldehyde have been calculated as 1.21968 Å and 1.11594 Å, respectively. Next, we considered different adsorption modes of formaldehyde on TiO_2 (0 0 1) surface. Generally, various adsorption modes are available for a single molecule to either interact physically or chemically with the catalyst surface depending on the molecular structure, molecular weight, temperature, and surface features [43,44]. Fig. 3 demonstrates various adsorption modes for the formaldehyde molecules studied in this work. In FDH_A, the calculated bond length between ═O of formaldehyde and Ti_{5c} is 2.411 Å, while the nearest distance for H to O_{2c} on the surface is measured as 2.3696 Å. Consequently, the C═O bond in formaldehyde increases to 1.229 Å, which shows a 9.73% increase in contrast to C═O bond length in the gas phase (1.115 Å). Likewise, the Ti_{5c}−O_{2c} bond length increases to 1.913 Å on the site where hydrogen is interacting with O_{2c} signifying a strong interaction between H and O_{2c} in contrast to ═O−Ti_{5c}. Moreover, the calculated E_{ads} value (0.351 eV) given in Table 1 recommends a physical adsorption between the formaldehyde molecule and TiO_2 (0 0 1) surface. In FDH_B, the ═O−Ti_{5c} bond length is measured as 2.449 Å while the H−O_{2c} bond distance is 2.126 Å. In contrast to FDH_A, the C−H bond in formaldehyde is observed to increase (1.108 Å) confirming more interaction between formaldehyde molecule through H with O_{2c} on TiO_2 (0 0 1) surface. In FDH_C and FDH_E, we assessed bonded configurations of formaldehyde molecule connected through ═O−Ti_{5c} and H−O_{2c} bonds, respectively. The molecules are initially attached to TiO_2 (0 0 1) surface through chemical bonds in these configurations; however, the respective bonds elongate during simulations, which negate the formation of chemical bonds on predetermined sites. It can be seen in FDH_C and FDH_E, that the

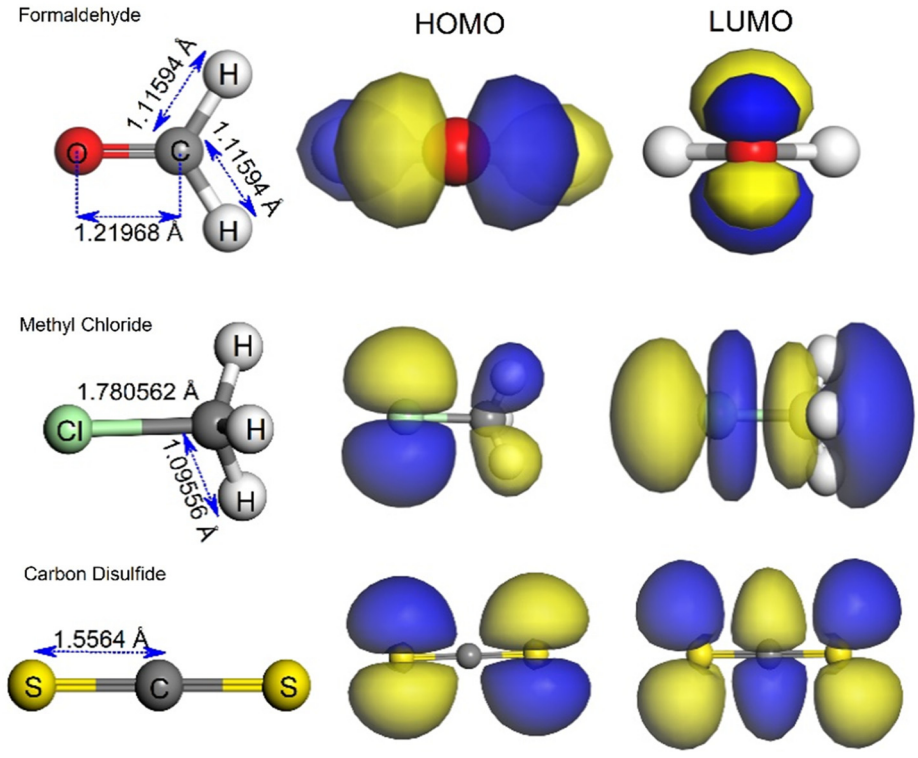

Fig. 2. Geometrically optimized structures and corresponding HOMO, LUMO orbitals for formaldehyde, methyl chloride and carbon disulfide in the gas phase. The carbon and hydrogen atoms are colored in dark and light grey respectively. The oxygen, chlorine, and sulfur atoms are colored as red, green, and yellow respectively. The bond length is given in Å.

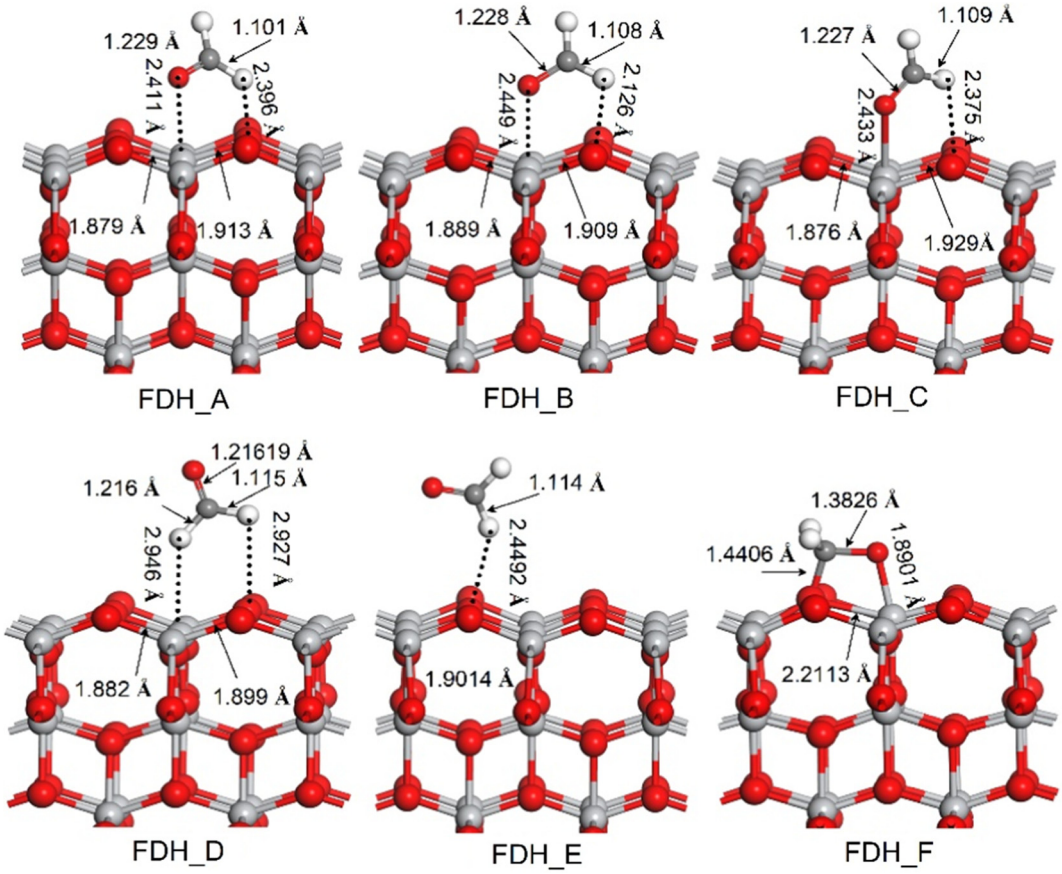

Fig. 3. Optimized geometries of formaldehyde on anatase TiO_2 (0 0 1) surface. The carbon and hydrogen atoms of formaldehyde are colored in dark gray and white, while oxygen and titanium atoms are colored in red and light gray, respectively. The number demonstrates the calculated bond length (unit: Å).

Table 1
Calculated adsorption energies of formaldehyde, methyl chloride, and carbon disulfide on TiO_2 (0 0 1) surface.

Mode	E_{ads} (eV)		
	FDH	MTC	CDS
A	0.351	0.143	0.226
B	0.298	0.208	0.108
C	0.317	0.193	0.0429
D	0.0018	0.215	0.0567
E	0.0642	0.165	0.237
F	0.543	0.251	–

calculated bond values do not tally to a chemical adsorption mode for the formaldehyde molecule on the TiO_2 (0 0 1) surface. For example, the $=O-Ti_{5c}$ bond (2.433 Å) value is even higher than the value observed for the same bond in FDH_A, which is 2.411 Å. Similarly, a small change can be seen in the C=O distance in contrast to FDH_A and FDH_B. A weak interaction for the H in formaldehyde and the surface can be seen in FDH_D configuration. Furthermore, no significant structural variations can be observed in this configuration suggesting a weak interaction. In contrast to above mentioned interactions, FDH_F configuration presents a saddle like structure. The molecule is chemically attached to TiO_2 (0 0 1) surface through $C-O_{2c}$ and $=O-Ti_{5c}$ bonds. The corresponding adsorption energies for various configurations suggest FDH_F as the most stable adsorption mode of formaldehyde on TiO_2 (0 0 1) surface exhibiting an adsorption energy value of 0.65 eV. Therefore, in the next section, we will only discuss FDH_F mode of adsorption.

The structural deformation can be clearly seen in FDH_F on the surface as well as in the formaldehyde structure. The O_{2c} atom is completely pulled out from the surface, which results in the formation of a new bond between C in formaldehyde and O_{2c} on the surface of TiO_2 (1.4406 Å). Consequently, the O_{2c} and Ti_{5c} bond length (2.2113 Å) increases by 16.19%, in contrast to 1.88 Å of the clean TiO_2 (0 0 1) surface after adsorption. Furthermore, the $=O-Ti_{5c}$ new bond distance is calculated as 1.8901 Å, which is almost the same as $Ti_{5c}-O_{2c}$ bond length. The C=O bond length in formaldehyde increases to 1.3826 Å (12.52%) compared to 1.21968 Å in the gas phase. Among the various adsorption modes studied, the FDH_F mode exhibited a saddle like structure causing distortion in the structure and exhibiting a high value of adsorption energy. Such kinds of structures have been previously reported for the molecules on the surface of TiO_2 [45–47]. This study suggests that FDH_F configuration is the most probable mode of adsorption and the formaldehyde is chemically adsorbed through chemical bond formation via $C-O_{2c}$ and $=O-T_{5c}$ bonds on the TiO_2 (0 0 1) surface. This renders stability to the chemically adsorbed molecule. The formation of FDH_F complex is an exothermic process, and some new bonds such as $C-O_{2c}$, $=O-Ti_{5c}$ are formed, indicating that anatase TiO_2 (0 0 1) surface can effectively adsorb and capture formaldehyde on its surface.

We further calculated the LDOS and electron density difference for the FDH_F complex to contemplate the adsorption mechanism in depth. Only the most stable adsorption mode has been considered in these calculations. The LDOS peaks can be successfully used to comprehend the interaction between the two connected atoms. The total LDOS for the formaldehyde molecule attached to TiO_2 (0 0 1) surface layer is given in Fig. 4, including the PDOS for Ti_{5c}, O_{2c}, =O, C, and H. Additionally, PDOS for the clean surface and formaldehyde molecule in the gas phase are also given (Fig. 4f and g). The total LDOS for the TiO_2 (0 0 1) surface and molecule demonstrate that s, p, and d-states are the

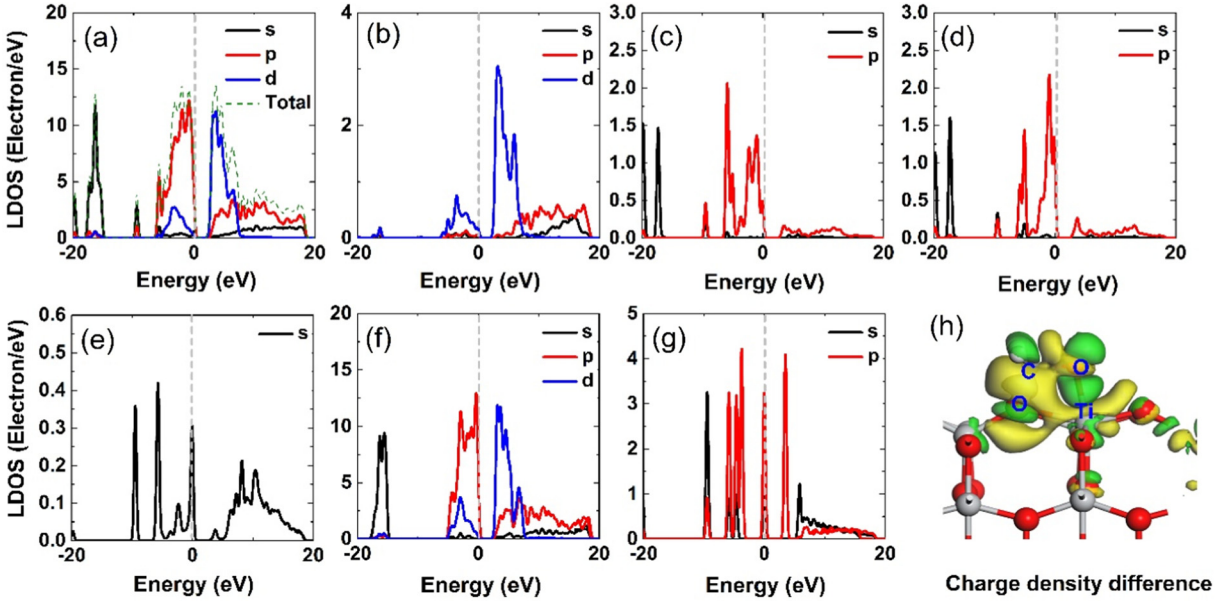

Fig. 4. Local density of states: (a) anatase TiO_2 (0 0 1) surface and formaldehyde molecule, (b) Ti_{5c}, (c) O_{2c}, (d) =O of formaldehyde, (e) hydrogen, (f) TiO_2 (0 0 1) surface before adsorption, (g) formaldehyde molecule in the gas phase. The Fermi energies are set as 0 eV. (h) Charge density difference for the FDH_F complex.

only contributors. It is observed that O_{2c} and =O 2p-states mainly contribute to the valence band (VB) while a small contribution in the conduction band (CB) can also be seen from the 2p-states. This behavior can be clearly distinguished using PDOS for O_{2c} and =O (Fig. 4c and d). The O_{2c} and =O 2p-states demonstrate sharp peaks in the upper VB. The sharp peaks for the formaldehyde molecule in the gas phase exhibit a typical behavior of a molecule (Fig. 4g). The contribution of O_{2c} 2p-states can be observed around −4.18 to 0 eV while the =O 2p-states demonstrate contribution from −10.25 to 0 eV. The O_{2c} 2p-states are significantly different in shape and intensity prior to bonding (in clean surface), which confirms the C−O_{2c} bond formation. The Ti_{5c} 3d-states are contributing more in the lower CB from 7.76 to 2.49 eV while comparatively small contributions can also be traced around −4.9 to 0 eV in the VB. The Ti_{5c} 4s and H 1s-states mainly contribute in the CB and only a small contribution can be seen from =O 2s-states in the VB. The intensity and shape of =O 2p states and Ti_{5c} 3d-states significantly change in contrast to =O and Ti_{5c} in the gas phase molecule and clean surface, respectively, which evidences the coupling between these two states. Additionally, the corresponding Ti_{5c} 3d and =O 2p-states broaden, which is a characteristic coupling behavior. Based on these results, we can conclude a chemical bond formation between the formaldehyde molecule and TiO_2 (0 0 1) surface. These results are in good agreement with the adsorption studies discussed previously in this paper. Next, we studied the charge density difference for the FDH_F complex structure. The green part demonstrates electron-rich region and the yellow part shows the electron depleting area. In the current scenario, it is clear that =O−Ti_{5c} and C−O_{2c} exhibit the highest charge density regions. The increasing charge density around the bonded region shows the bond's strength. In contrast, the interaction between the surface Ti_{5c} and O_{2c} is rather weak. Thus, the surface oxygen prefers to form a bond with the C formaldehyde and so on for the Ti_{5C} and −O interaction. This study is in good agreement with the optimized adsorption mechanism study.

3.3. Methyl chloride (MTC) adsorption

Fig. 5 shows various adsorption modes including MTC_A to MTC_F demonstrating methyl chloride adsorption on TiO_2 (0 0 1) surface. It can be observed that adsorption of methyl chloride does not cause any structural deformation in TiO_2 (0 0 1) surface in all cases. However, the methyl chloride molecule significantly reorients from the initial position (not shown) to a stable geometry during computations. In MTC_A, the Cl−Ti_{5c} bond length is calculated as 3.0805 Å suggesting a physical adsorption. This value is observed to slightly change for different adsorption modes studied in this work. The MTC_F configuration, where methyl chloride is interacting with TiO_2 (0 0 1) surface through Cl and H exhibits the highest adsorption energy (0.251 eV) in contrast to other configurations (Table 1). In MTC_A, the Cl−Ti_{5c} bond length is calculated as 3.0805 Å, which can be inferred to be a physical interaction. A slight increase in the Ti_{5c}−O_{2c} (1.89454 Å) can be seen; however, no chemical bond formation can be traced on TiO_2 (0 0 1) surface. Similarly, the C−Cl bond in MTC_A molecule is measured to be 1.7832 Å, which increases slightly (0.148%) than C−Cl bond (1.780562 Å) for the same molecule in the gas phase. The Cl−Ti_{5c} interaction can only be traced in MTC_A, MTC_D, and MTC_F. As stated earlier, the Cl−Ti_{5c} bond length in MTC_A (3.0805 Å) is shorter than Cl−Ti_{5c} bond in MTC_D (3.5389 Å) and MTC_F (3.3199 Å). However, the Cl−O_{2c} bond length in MTC_B is smaller (3.0628 Å) than Cl−Ti_{5c} bond by 0.58%. The H−O_{2c} bond can be seen in MTC_C and MTC_F. The H−O_{2c} bond length in MTC_F (2.5554 Å) is smaller than H−O_{2c} bond in MTC_C (2.9595 Å) suggesting a strong interaction of methyl chloride via H−O_{2c} on TiO_2 (0 0 1) surface. Based on adsorption energy values for different configurations, the MTC_F unexpectedly demonstrates the highest adsorption energy. Thus, it can be inferred that methyl chloride weakly adsorbs to the surface using Cl−Ti_{5c} and H−O_{2c} interactions following a physical adsorption mechanism on TiO_2 (0 0 1) surface. Additionally, no chemically adsorbed stable complex can be observed for all the methyl chloride orientations in this study.

Therefore, we will discuss the highest adsorption energy complex (MTC_F) in the following, which demonstrates the most probable adsorption mechanism for methyl chloride on TiO_2 (0 0 1) surface. The molecular structure suggests that methyl chloride can adsorb on TiO_2 (0 0 1) surface through four possible ways: Cl−Ti_{5c}, H−O_{2c}, Cl−O_{2c}, and C−O_{2c}. We ruled out the C−O_{2c} attachment because the C atom is surrounded by three hydrogens, which for the most part makes it impossible for methyl chloride to interact with TiO_2 (0 0 1) surface through this C atom. Moreover, no obvious distortion or a saddle like structure formation occurs during these adsorption modes. However, In the MTC_F configuration, the Ti_{5c}−O_{2c} bond length increases (0.73%) to 1.8937 Å from the original value of 1.88 Å in the clean surface. Similarly, the C−Cl bond length (1.7826 Å) in methyl chloride increases

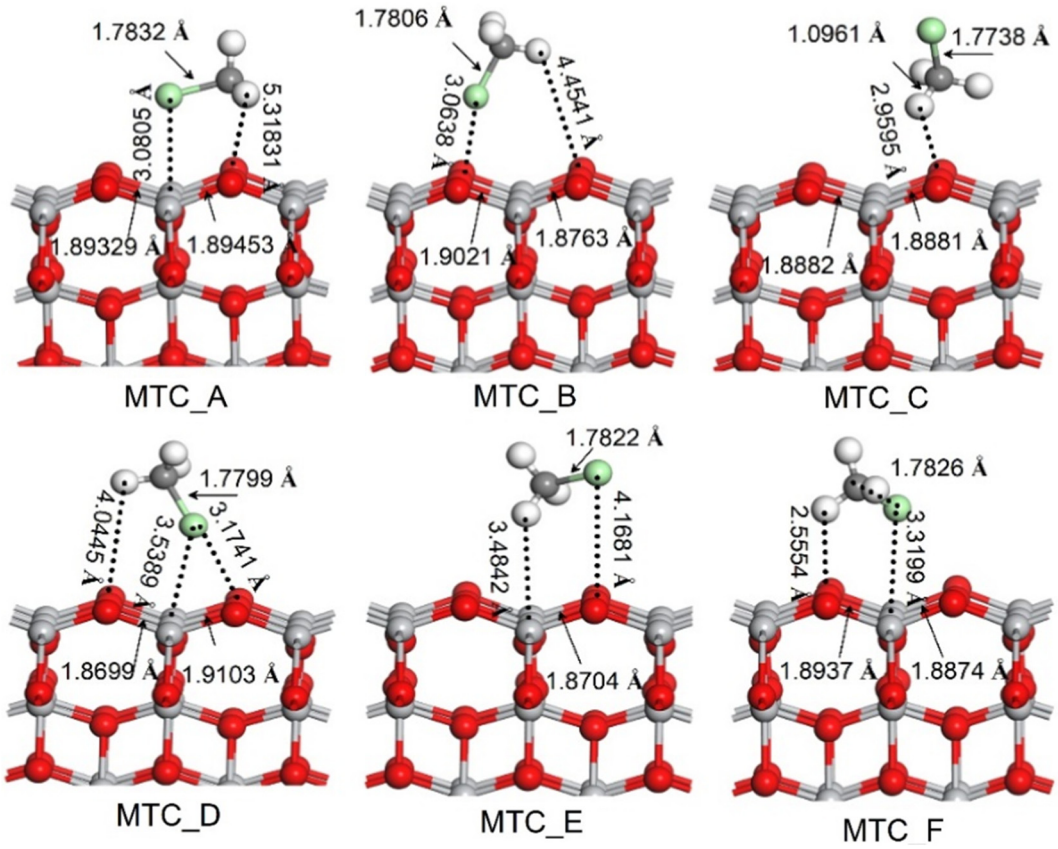

Fig. 5. Optimized geometries of methyl chloride on anatase TiO_2 (0 0 1) surface. The carbon and hydrogen atoms of formaldehyde are colored in dark gray and white, the chlorine atom is colored green, while oxygen and titanium atoms are colored in red and light gray, respectively. The number demonstrates the calculated bond length (unit: Å).

by 0.12% in contrast to the gas phase (Fig. 2). The small adsorption values (less than 0.6 eV) for different methyl chloride adsorption modes suggest physical adsorption of methyl chloride on the TiO_2 (0 0 1) surface. Our study suggests that Cl interaction with Ti_{5c} and O_{2c}, and H interaction with the O_{2c} contribute to some extent to the physical adsorption of methyl chloride on TiO_2 (0 0 1) surface.

The total LDOS of methyl chloride attached to the TiO_2 (0 0 1) surface layer is given in Fig. 6a, including PDOS for the Ti_{5c}, O_{2c}, Cl, and H of methyl chloride. Additionally, the clean surface and molecule in the gas phase are also given in Fig. 6f and g, respectively. The data shows that the VB is mainly contributed by 2p-states of O_{2c} and 3p-states of Cl (−4.7 to 0 eV) (Fig. 6a). Additionally, the 3d-states of Ti_{5c} weakly contribute to the upper VB. To further evaluate the contribution of individual atoms, we calculated the PDOS. In Fig. 6b, the 3d-states of Ti_{5c} demonstrate a broad peak in the CB around 2.22 to 7.5 eV. In addition, the 3d-states of Ti_{5c} also contribute in the upper VB at around −5.2 to 0 eV. A small contribution from the Ti_{5c} 4s-states can be seen in the upper CB at approximately 7.5 to 18 eV. The 2p-states of O_{2c} mainly contribute at around −4.17 to 0 eV exhibiting a broad peak in contrast to two small peaks (−1 to 0 eV; and −4.7 to 3.4 eV) in the same region by 3p-states of Cl. The peaks intensity of the 3d-states in the clean surface (Fig. 6f) significantly decreases after adsorption of methyl chloride, which suggests an interaction between methyl chloride and the surface. Similarly, the 3p-states of Cl at around −4.7 to 3.4 eV changes predominantly in the adsorption complex in contrast to the pure 3p-states in the gas phase (Fig. 6g). Similarly, the hydrogen 1s states decrees in intensity suggesting stronger coupling in contrast to Cl. However, based on the adsorption energy values, this interaction can only be regarded as the physical adsorption and no chemical adsorption or chemical bond formation can be traced for the methyl chloride on the surface of TiO_2 (0 0 1). We further calculated the electron density difference for MTC_F complex to evaluate the adsorption mechanism (Fig. 6h). It is observed that Cl and O_{2c} are gaining more electrons in contrast to other regions. Similarly, the Ti_{5c} and hydrogen sites are the electron depleting regions. The electron density appears to be transferred to the sites where methyl chloride is interacting with TiO_2 (0 0 1) surface. Our adsorption study comprehends the interaction between Cl—Ti_{5c} and H—O_{2c} and the electron density difference study reflects the same behavior.

3.4. Carbon disulfide (CDS) adsorption

Fig. 7 show adsorption of carbon disulfide on TiO_2 (0 0 1) surface. The carbon disulfide atom contains two sulfur atoms attached to the carbon through two double bonds (1.5664 Å) (Fig. 2). It can be inferred that carbon disulfide will attach to TiO_2 (0 0 1) surface either through sulfur or carbon atom [48]. It is observed from CDS_A that the calculated bond length between S and O_{2c} is 3.092 Å; however, no structural deformation can be traced on the surface nor in the carbon disulfide structure suggesting a weak interaction in this adsorption mode. For instance, the bond length of S and C is measured as 1.557 Å, which is almost the same as in the gas phase. The closest bond distance between the S and O_{2c} in CDS_A and CDS_B is measured as 3.298 and 3.65 Å, respectively. In all these configurations, no chemical bond formation can be seen. In CDS_E, a structural deformation can be clearly seen suggesting a strong interaction between the carbon disulfide molecule and TiO_2 (0 0 1) surface. The calculated adsorption energies for various carbon disulfide adsorption modes on TiO_2 (0 0 1) is given in Table 1. The corresponding E_{ads} values suggest that CDS_E exhibit the highest adsorption energy (E_{ads} = 0.237 eV) among the various adsorption modes studied in this work. The bond distance between S and Ti_{5c} is measured as 2.717 Å. Additionally, the oxygen atom from the surface is

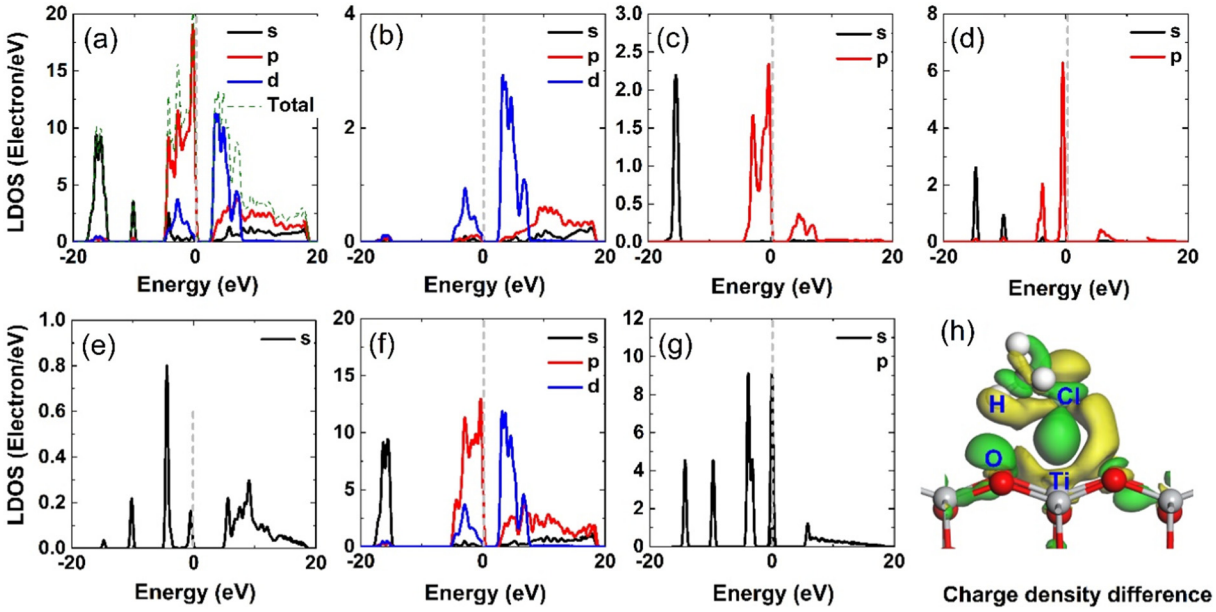

Fig. 6. Local density of states: (a) anatase TiO_2 (0 0 1) surface and methyl chloride molecule, (b) Ti_{5c}, (c) O_{2c}, (d) Cl of methyl chloride, (e) hydrogen, (f) TiO_2 (0 0 1) surface before adsorption, (g) methyl chloride molecule in the gas phase. The Fermi energies are set as 0 eV. (h) Charge density difference for the MTC_F complex.

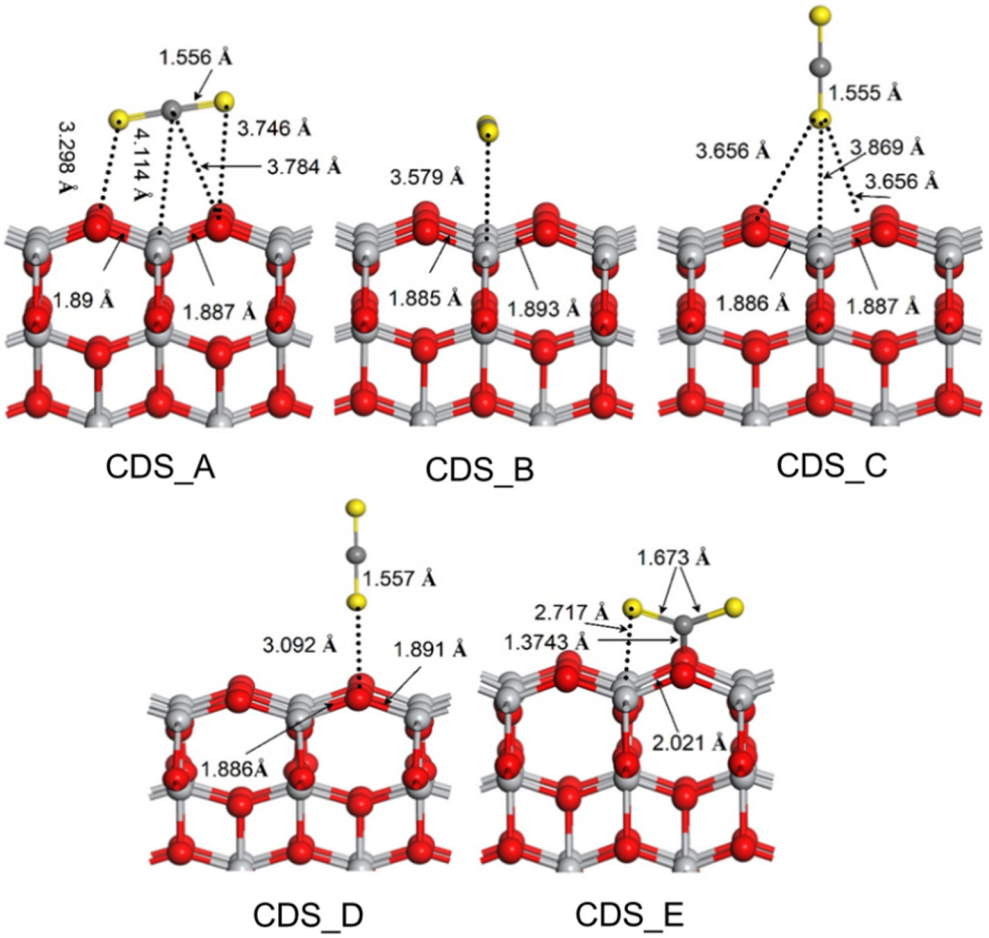

Fig. 7. Optimized geometries of carbon disulfide on anatase TiO_2 (0 0 1) surface. The carbon and sulfur atoms of carbon disulfide are colored in dark gray and yellow, while oxygen and titanium atoms are colored in red and light gray, respectively. The number demonstrates the calculated bond length (unit: Å).

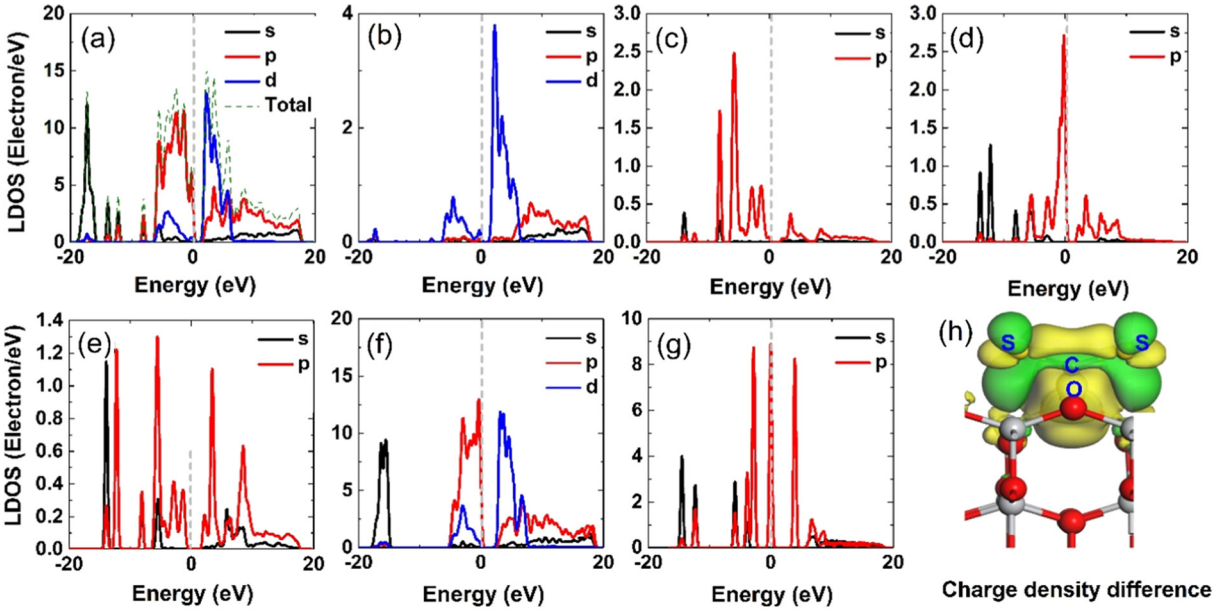

Fig. 8. Local density of states: (a) anatase TiO_2 (0 0 1) surface and carbon disulfide molecule, (b) Ti_{5c}, (c) O_{2c}, (d) S of carbon disulfide, (e) C of carbon disulfide, (f) TiO_2 (0 0 1) surface before adsorption, (g) carbon disulfide molecule in the gas phase. The Fermi energies are set as 0 eV. (h) Charge density difference for the CDS_E complex.

pulled out to some extent, which results in the formation of strong attachment in the form of C—O_{2c} (1.3743 Å). Moreover, the C═S double bond increases (7.22%) in length to 1.673 Å, which has been recorded as 1.5564 Å in the gas phase. It is clear in CDS_E that the S atoms in the molecule bend upward from the surface making an angle of 136.43° among S═C═S atoms. A significant increase (6.91%) in the Ti_{5c}—O_{2c} bond length can also be seen. This kind of adsorption model has been previously proposed by Clark et al. [49] in their experimental study. Despite this strong interaction, the adsorption energy of CDS_E and CDS_A are almost the same, where CDS_A demonstrates an interaction between the S atoms of molecules with O_{2c} on TiO_2 (0 0 1) surface. Based on these results, it can be inferred that there is no chemical bond formation between the carbon disulfide molecule and TiO_2 (0 0 1) surface, which is evidenced from the low adsorption energy values for all the configurations. However, the adsorption mode in which C atom of carbon disulfide is attached to O_{2c} and S atoms are attracting to Ti_{5c} renders more stability to the complex in contrast to other configurations. Sui et al. [50] proposed that a hydroxide group present on the TiO_2 surface will play a major role to chemically adsorb the carbon disulfide in order to form a Lewis acid-Lewis base interaction. The highest adsorption energy calculated for the CDS_E recommend it as the possible adsorption mechanism for the carbon disulfide molecule on TiO_2 (0 0 1) surface.

Fig. 8 shows the LDOS of carbon disulfide molecule attached to TiO_2 (0 0 1) surface for the CDS_E model structure. It is clear that LDOS is contributed by s, p, and d states, only. To further contemplate the individual contribution by each element and their corresponding states, we calculated the PDOS for Ti_{5c}, O_{2c}, S, C, and the surface atomic layer of clean TiO_2 (0 0 1) and molecule in the gas phase. The 2p-states of O_{2c}, S, and C mainly contribute to the high VB (−6.176 to 0 eV). As stated earlier the sharp peaks of the S and C in the gas phase significantly decrease in intensity, while the width of the peaks also increases in size. This behavior confirms the strong interaction between the S, C, of carbon disulfide to Ti_{5c} and O_{2c} on TiO_2 (0 0 1) surface., respectively. The 3d-states of Ti_{5c} states mainly contribute in the lower CB. The intensity of this contribution is high in the clean surface (TiO_2 (0 0 1) surface (Fig. 8f), however, it demonstrates a significant decrease in the Fig. 8b, suggesting a coupling between the surface and Ti_{5c}. The O_{2c} peaks in (Fig. 8c) predominantly sharpens in contrast to broad peaks in Fig. 8f, which confirms the interaction between the carbon atom and O_{2c}. We further studied the electron density difference for the CDS_E complex. The electron density mainly surrounds S, Ti_{5c}, C, and O_{2c}. This result suggests that there a strong coupling among these atoms which further confirms the adsorption and LDOS results.

4. Conclusion

In summary, we have successfully implemented the first principle calculations to study the adsorption mechanism of three VOCs including formaldehyde, methyl chloride, and carbon disulfide on the surface of TiO_2 (0 0 1) in detail. In addition, the local density of states and partial density of states were studied to further understand and confirm the coupling between different atomic orbitals. Different orientations of molecules on the TiO_2 (0 0 1) surface have been studied to trace the most possible adsorption mechanism. The results suggest that Ti_{5c} and O_{2c} are the potential adsorption sites on the surface of TiO_2 which trap the VOCs molecules. However, different molecules exhibiting different functional groups interact very differently with the surface, therefore, it is of utmost importance to study the molecules chemical structure and possible affinity with the catalysts surface before designing the catalyst. For instance, the formaldehyde molecule adsorbs to the surface through the formation of a saddle like structure between the ═O and C of the formaldehyde molecule with the Ti_{5c} and O_{2c} of the TiO_2 (0 0 1) surface, respectively. However, in contrast, the methyl chloride molecule only weakly bounds to the surface and no chemical bond formation can be traced suggesting a physical adsorption. Also, the carbon disulfide molecule did not show a strong affinity towards the (0 0 1) surface of TiO_2. Therefore, it can be concluded that the aldehyde group in formaldehyde demonstrate a strong affinity to TiO_2 (0 0 1) surface in contrast to methyl and sulfide groups.

Acknowledgement

The authors are thankful for the financial support under the CAS President's International Fellowship Initiative (PIFI) program, National Key Research and Development Program of China (2016YFA0203000), Shanghai International Cooperation Program (17520742600).

Appendix A. Supplementary material

Supplementary data to this article can be found online at https://doi.org/10.1016/j.apsusc.2018.12.017.

References

[1] K.L. Pan, G.T. Pan, S. Chong, M.B. Chang, Removal of VOCs from gas streams with double perovskite-type catalysts, J. Environ. Sci. (China) 69 (2018) 205–216.
[2] B. Wang, S. Yao, Y. Peng, Y. Xu, Toluene removal over TiO_2-$BaTiO_3$ catalysts in an atmospheric dielectric barrier discharge, J. Environ. Chem. Eng. 6 (2018) 3819–3826.
[3] L. Hui, X. Liu, Q. Tan, M. Feng, J. An, Y. Qu, Y. Zhang, M. Jiang, Characteristics, source apportionment and contribution of VOCs to ozone formation in Wuhan Central China, Atmos. Environ. 192 (2018) 55–71.
[4] C.Y. Hsu, H.C. Chiang, R.H. Shie, C.H. Ku, T.Y. Lin, M.J. Chen, N.T. Chen, Y.C. Chen, Ambient VOCs in residential areas near a large-scale petrochemical complex: spatiotemporal variation, source apportionment and health risk, Environ. Pollut. 240 (2018) 95–104.
[5] W. Hong-Li, J. Sheng-Ao, L. Sheng-Rong, H. Qing-Yao, L. Li, T. Shi-Kang, H. Cheng, Q. Li-Ping, C. Chang-Hong, Volatile organic compounds (VOCs) source profiles of on-road vehicle emissions in China, Sci. Tot. Environ. 607–608 (2017) 253–261.
[6] M.A. Bari, W.B. Kindzierski, Ambient volatile organic compounds (VOCs) in Calgary, Alberta: sources and screening health risk assessment, Sci. Tot. Environ. 631–632 (2018) 627–640.
[7] J. Chen, X. Chen, X. Chen, W. Xu, Z. Xu, H. Jia, J. Chen, Homogeneous introduction of CeOy into MnO*x* -based catalyst for oxidation of aromatic VOCs, Appl. Catal. B: Environ. 224 (2018) 825–835.
[8] M.I. Swasy, M.L. Campbell, B.R. Brummel, F.D. Guerra, M.F. Attia, G.D. Smith, F. Alexis, D.C. Whitehead, Poly(amine) modified kaolinite clay for VOC capture, Chemosphere 213 (2018) 19–24.
[9] L.-H. Xie, X.-M. Liu, T. He, J.-R. Li, Metal-organic frameworks for the capture of trace aromatic volatile organic compounds, Chem 4 (2018) 1911–1927.
[10] M. Zhu, P. Hu, Z. Tong, Z. Zhao, Z. Zhao, Enhanced hydrophobic MIL(Cr) metal-organic framework with high capacity and selectivity for benzene VOCs capture from high humid air, Chem. Eng. J. 313 (2017) 1122–1131.
[11] M. Modesti, M. Roso, C. Boaretti, S. Besco, D. Hrelja, P. Sgarbossa, A. Lorenzetti, Preparation of smart nano-engineered electrospun membranes for methanol gas-phase photoxidation, Appl. Catal. B: Environ. 144 (2014) 216–222.
[12] J. Lyu, J. Gao, M. Zhang, Q. Fu, L. Sun, S. Hu, J. Zhong, S. Wang, J. Li, Construction of homojunction-adsorption layer on anatase TiO_2 to improve photocatalytic mineralization of volatile organic compounds, Appl. Catal. B: Environ. 202 (2017) 664–670.
[13] G. Zhou, H. Lan, T. Gao, H. Xie, Influence of Ce/Cu ratio on the performance of ordered mesoporous CeCu composite oxide catalysts, Chem. Eng. J. 246 (2014) 53–63.
[14] C. He, B.-T. Xu, J.-W. Shi, N.-L. Qiao, Z.-P. Hao, J.-L. Zhao, Catalytic destruction of chlorobenzene over mesoporous ACeO*x* (A = Co, Cu, Fe, Mn, or Zr) composites prepared by inorganic metal precursor spontaneous precipitation, Fuel Process. Technol. 130 (2015) 179–187.
[15] Y. Shu, Y. Xu, H. Huang, J. Ji, S. Liang, M. Wu, D.Y.C. Leung, Catalytic oxidation of VOCs over Mn/TiO_2/activated carbon under 185nm VUV irradiation, Chemosphere 208 (2018) 550–558.
[16] J. Hu, W.B. Li, R.F. Liu, Highly efficient copper-doped manganese oxide nanorod catalysts derived from CuMnO hierarchical nanowire for catalytic combustion of VOCs, Catal. Today 314 (2018) 147–153.
[17] J.-J. Li, E.-Q. Yu, S.-C. Cai, X. Chen, J. Chen, H.-P. Jia, Y.-J. Xu, Noble metal free, CeO_2/$LaMnO_3$ hybrid achieving efficient photo-thermal catalytic decomposition of volatile organic compounds under IR light, Appl. Catal. B: Environ. 240 (2019) 141–152.
[18] J.-O. Jo, Q.H. Trinh, S.H. Kim, Y.S. Mok, Plasma-catalytic decomposition of nitrous oxide over γ-alumina-supported metal oxides, Catal. Today 310 (2018) 42–48.
[19] Q. Zhang, S. Yuan, B. Xu, Y. Xu, K. Cao, Z. Jin, C. Qiu, M. Zhang, C. Su, T. Ohno, A facile approach to build $Bi_2O_2CO_3$/PCN nanohybrid photocatalysts for gaseous acetaldehyde efficient removal, Catal. Today 315 (2018) 184–193.
[20] W. Wang, C. Lu, Y. Ni, Z. Xu, Crystal facet growth behavior and thermal stability of 001 faceted anatase TiO2: mechanistic role of gaseous HF and visible-light photocatalytic activity, CrystEngComm 15 (2013) 2537.
[21] H. Wang, J.P. Lewis, Second-generation photocatalytic materials: anion-doped TiO_2, J. Phys.: Condensed Matter 18 (2006) 421–434.
[22] Amy L. Linsebigler, Lu. Guangquan, J. John, T. Yates, Photocatalysis on TiO_2 surfaces: principles, mechanisms, and selected results, Chem. Rev. 95 (1995) 735–758.
[23] X. Chen, S.S. Mao, Titanium dioxide nanomaterials: synthesis, properties, modifications, and applications, Chem. Rev. 107 (2007) 2891–2959.
[24] T. Luttrell, S. Halpegamage, J. Tao, A. Kramer, E. Sutter, M. Batzill, Why is anatase a better photocatalyst than rutile?–model studies on epitaxial TiO2 films, Sci. Rep. 4 (2014) 4043.
[25] R. Ren, Z. Wen, S. Cui, Y. Hou, X. Guo, J. Chen, Controllable synthesis and tunable photocatalytic properties of Ti(3+)-doped TiO_2, Sci. Rep. 5 (2015) 10714.
[26] J. Pan, G. Liu, G.Q. Lu, H.M. Cheng, On the true photoreactivity order of 001}, {010}, and {101 facets of anatase TiO2 crystals, Angew. Chem. 50 (2011) 2133–2137.
[27] M.-Y. Xing, B.-X. Yang, H. Yu, B.-Z. Tian, S. Bagwasi, J.-L. Zhang, X.-Q. Gong, Enhanced photocatalysis by Au nanoparticle loading on TiO_2 single-crystal (001) and (110) facets, J. Phys. Chem. Lett. 4 (2013) 3910–3917.
[28] Adawiya J. Haider, Riyad Hassan AL-Anbari, Ghadah Rasim Kadhim, C.T. Salame, Exploring potential environmental applications of TiO_2 nanoparticles, Energy Procedia 119 (2017) 332–345.
[29] T. Verdier, M. Coutand, A. Bertron, C. Roques, Antibacterial activity of TiO_2 photocatalyst alone or in coatings on E. coli: the influence of methodological aspects, Coatings 4 (2014) 670–686.
[30] M.M. Ba-Abbad, Amir H. Abdul, Abu Bakar Kadhum, Mohd S. Mohamad, K. Sopian Takriff, Synthesis and catalytic activity of TiO_2 nanoparticles for photochemical oxidation of concentrated chlorophenols under direct solar radiation, Int. J. Electrochem. Sci. 7 (2012) 4871–4888.
[31] D. Trivedi, J. Crosse, J. Tanti, A.J. Cass, K.E. Toghill, The electrochemical determination of formaldehyde in aqueous media using nickel modified electrodes, Sens. Actuat. B: Chem. 270 (2018) 298–303.
[32] K.Z. Gaca-Zając, B.R. Smith, A. Nordon, A.J. Fletcher, K. Johnston, J. Sefcik, Investigation of IR and Raman spectra of species present in formaldehyde-water-methanol systems, Vibrat. Spectrosc. 97 (2018) 44–54.
[33] M. Hirata, M. Ikeda, F. Fukuda, M. Abe, H. Sawada, S. Hashimoto, Effect of temperature on the production rates of methyl halides in cultures of marine proteobacteria, Mar. Chem. 196 (2017) 126–134.
[34] J. Llorens, Toxic neurofilamentous axonopathies-accumulation of neurofilaments and axonal degeneration, J. Internal Med. 273 (2013) 478–489.
[35] T. Goen, A. Schramm, T. Baumeister, W. Uter, H. Drexler, Current and historical individual data about exposure of workers in the rayon industry to carbon disulfide and their validity in calculating the cumulative dose, Int. Arch. Occupat. Environ. Health 87 (2014) 675–683.
[36] T. Venet, M. Carreres-Pons, M. Chalansonnet, A. Thomas, L. Merlen, H. Nunge, E. Bonfanti, F. Cosnier, J. Llorens, P. Campo, Continuous exposure to low-frequency noise and carbon disulfide: combined effects on hearing, Neurotoxicology 62 (2017) 151–161.
[37] John P. Perdew, Kieron Burke, M. Ernzerhof, Generalized gradient approximation made simple, Phys. Rev. Lett. 77 (1996) 3865–3868.
[38] C. Arrouvel, Effects of PH_2O, PH_2S, PH_2 on the surface properties of anatase TiO_2 and Al_2O_3: a DFT study, J. Catal. 226 (2004) 260–272.
[39] A. Hemeryck, A. Motta, C. Lacaze-Dufaure, D. Costa, P. Marcus, DFT-D study of adsorption of diaminoethane and propylamine molecules on anatase (101) TiO_2 surface, Appl. Surf. Sci. 426 (2017) 107–115.
[40] S. Grimme, Semiempirical GGA-type density functional constructed with a long-range dispersion correction, J. Comput. Chem. 27 (2006) 1787–1799.
[41] E. Araujo-Lopez, L.A. Varilla, N. Seriani, J.A. Montoya, TiO_2 anatase's bulk and (001) surface, structural and electronic properties: a DFT study on the importance of Hubbard and van der Waals contributions, Surf. Sci. 653 (2016) 187–196.
[42] M. Yao, Y. Ji, H. Wang, Z. Ao, G. Li, T. An, Adsorption mechanisms of typical carbonyl-containing volatile organic compounds on anatase TiO_2 (001) surface: a DFT investigation, J. Phys. Chem. C 121 (2017) 13717–13722.
[43] X. Zhang, B. Gao, A.E. Creamer, C. Cao, Y. Li, Adsorption of VOCs onto engineered carbon materials: a review, J Hazard Mater. 338 (2017) 102–123.
[44] Y. Su, Z. Ao, Y. Ji, G. Li, T. An, Adsorption mechanisms of different volatile organic compounds onto pristine C_2N and Al-doped C_2N monolayer: a DFT investigation, Appl. Surf. Sci. 450 (2018) 484–491.
[45] Y. Lei, F. Niu, H. Mei, Q. Liu, C. Pan, W. Xiao, Adsorption and diffusion studies of an O adatom on anatase surfaces with first principles calculations, Comput. Mater. Sci. 63 (2012) 58–65.
[46] G. He, G. Pan, M. Zhang, Studies on the reaction pathway of arsenate adsorption at water-TiO_2 interfaces using density functional theory, J. Colloid Interf. Sci 364 (2011) 476–481.
[47] W. Liu, J.-G. Wang, X. Guo, W. Fang, M. Wei, X. Lu, L. Lu, Dissociation of methanol on hydroxylated TiO_2-B (100) surface: insights from first principle DFT calculation, Catal. Today 165 (2011) 32–40.
[48] L. Wang, Y. Guo, G. Lu, Effect of activated carbon support on CS_2 removal over coupling catalysts, J. Nat. Gas Chem. 20 (2011) 397–402.
[49] P.D. Clark, N.I. Dowling, M. Huang, Role of Ti^{3+} in CS_2 conversion over TiO_2 Claus catalyst, Appl. Catal. A: Gen. 489 (2015) 111–116.
[50] R. Sui, C.B. Lavery, D. Li, C.E. Deering, N. Chou, N.I. Dowling, R.A. Marriott, Improving low-temperature CS_2 conversion for the Claus process by using La(III)-doped nanofibrous TiO_2 xerogel, Appl. Catal. B: Environ. (2018).